# Experimental Identification Approaches for a PEM Water Electrolyzer

Michel Zasadzinski, Meziane Ait Ziane and Marouane Alma

***Abstract*— This paper focuses on the experimental identification of a proton exchange membrane water electrolyzer models. Two types of approaches are investigated: temporal and frequency domains identification techniques. The obtained models are validated and compared. A discussion is then provided to highlight the implications of using these identified models, particularly with respect to the choice of operating points, the impact of aging on model complexity, and their relevance for control and diagnostic purposes.**

## I. Introduction

Green hydrogen plays an important role in decarbonizing the industrial and transport sectors. This hydrogen is produced using Water Electrolyzers (WE) powered by low-carbon energy sources such as nuclear, wind or photovoltaic energy. The main WE technologies include Alkaline Water Electrolyzers (AWE), Anion Exchange Membrane Water Electrolyzers (AEMWE) and Proton Exchange Membrane Water Electrolyzers (PEMWE). AWE is a mature technology, widely used in industrial applications, but it presents some drawbacks, such as low current density and poor tolerance to the variability of renewable energy sources (RES) [1]. PEMWE technology provides the benefit of operating effectively with intermittent renewable energies and can handle high current densities, up to 2 A/cm$^2$ [2]. The main disadvantage of the PEMWE is that it is made from rare and expensive materials, particularly for the assembly electrode membrane. AEMWE technology aims to combines the advantages of AWE and PEMWE, but it is still under development [3].

Modeling such systems is a challenging task, due to strong nonlinear interactions of several physical phenomena (electrical, electrochemical, thermal, etc.). The modeling approach depends on the intended application. In the literature, control oriented models based on thermal, electrical and chemical relationships are available [4], [5], along with models based on equivalent electrical circuits [6], [7], [8], [9] which can be obtained using either temporal domain [10], [11], [12] or frequency domain [13], [14] approaches. Additionally, static models are proposed for energy management purposes in [15].

The identification of PEMWE models is addressed differently depending on the approach considered: electrical, physical or chemical. In this paper, PEMWE model identification is investigated on a PEMWE test bench using two approaches, time domain and frequency domain approaches. The objective is to obtain linear models that cover a wide range of PEMWE operating conditions and to discuss on some important consequences of the use of these identified models, particularly regarding the selection of operating points, the impact of aging on model complexity, and control/diagnosis purposes.

This paper is organized as follows. Section II is dedicated to experimental black box identification: the used test bench for the identification procedure is described in Section II-A, temporal domain approach is presented in Section II-B and frequency domain approach is detailed in Section II-C, Section II-D provides an analysis of the obtained models in terms of gap metric. Section III deals, on the one hand, with the analysis of the identified models, on the other hand, with open questions generated from this analysis with respect to PEMWE modeling, control and diagnosis. Finally, Section IV concludes the paper.

## II. Black box identification approaches

### A. Experimental test bench

The PEMWE stack is composed of 3-cell supplied by an Direct Current (DC) through an EA-PS-9080-100 device as shown in Fig. 1.

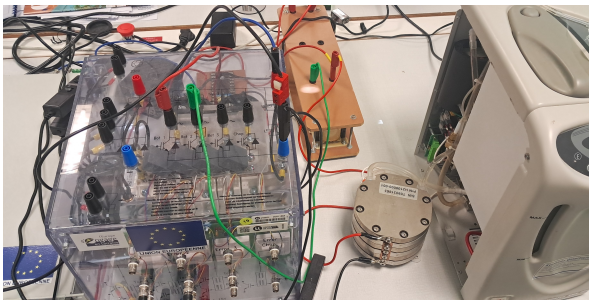

Fig. 1: Experimental test bench

Table I provides the characteristics of the PEMWE stack employed in this paper.

TABLE I: PEMWE stack technical specifications

| Parameters | Values | Units |
|---|---|---|
| Rated power | 400 | W |
| Cell number $N_c$ | 3 | $\times$ |
| Max current | 50 | A |
| Active area | 50 | cm$^2$ |

The polarization curve which describes the relation between the current $I$ and the voltage $V$ of the used PEMWE in this paper is shown in Fig. 2.

This work was not supported by any organization

M. Zasadzinski and Marouane Alma are with Research Center for Automatic Control of Nancy (CRAN), UMR CNRS 7039, Université de Lorraine, F-54000 Nancy, France michel.zasadzinski@univ-lorraine.fr, marouane.alma@univ-lorraine.fr

M. Ait Ziane is with Université de Lorraine, GREEN, F-54000 Nancy, France. meziane.ait-ziane@univ-lorraine.fr

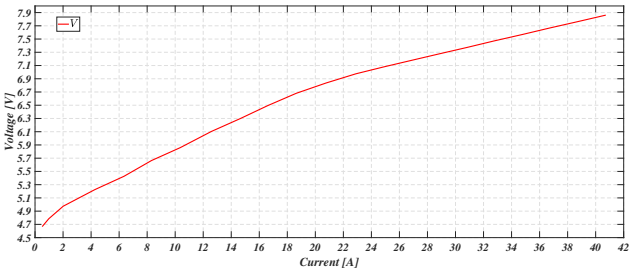


Fig. 2: PEMWE polarization curve

### B. Temporal domain approach

The objective of this section is to identify a relationship from the PEMWE current $I$ to the PEMWE voltage $V$. As shown in the polarization curve (see Fig. 2), the behavior of the PEMWE system is nonlinear. So, obtaining a linear model requires process identification arround several operating points. For each operating point, the transfer function $F_{d_j}(z)$ is expressed as

$$F_{d_j}(z) = \frac{N_{d_j}(z)}{D_{d_j}(z)} = \frac{b_{j_{n-1}} z^{n-1} + \ldots + b_{j_1} z + b_{j_0}}{z^n + a_{j_{n-1}} z^{n-1} + \ldots + a_{j_1} z + a_{j_0}} \tag{1}$$

where $b_{j_{n-1}}, \ldots, b_{j_0}$ and $a_{j_{n-1}}, \ldots a_{j_0}$ are the model parameters to be identified, and $j$ efers to the number of the considered operating point.

The transfer function given in (1) leads to the following input-output relationship in the $\mathcal{Z}$ domain:

$$\widehat{\mathcal{V}}_{d_j}(z) = F_{d_j}(z)\widetilde{\mathcal{I}}_{d_j}(z) \tag{2}$$

where $\widehat{\mathcal{V}}_{d_j}(z)$ and $\widetilde{\mathcal{I}}_{d_j}(z)$ denote the $\mathcal{Z}$-transforms of discrete-time signals $\widehat{V}_j$ and $\widetilde{I}_j$, respectively. The signals $\widetilde{V}_j$ and $\widetilde{I}_j$ are obtained by centering the raw input/output signals with respect to the $j^{\text{th}}$ operating point as follows

$$\widetilde{I}_{j_k} = I_k - I_0 \tag{3a}$$

$$\widetilde{V}_{j_k} = V_k - V_0 \tag{3b}$$

where $I$ and $V$ are the measured signals, $\widetilde{I}_{j_k} = 0$ and $\widetilde{V}_{j_k} = 0$ when $k \leqslant 0$. Here $k$ represents the sample number at the time sample $kT_s$. So, $\widehat{V}_j$ is considered as the the estimation of $\widetilde{V}_j$ obtained from (2). The estimation error $\mathcal{E}_j$ is defined as

$$\mathcal{E}_{j_k} = \widetilde{V}_{j_k} - \widehat{V}_{j_k} \tag{4}$$

This error can be minimized using the Output-Error (OE) identification methods as proposed in textbooks [16], [17] [18], [19]. Combining (1), (2) and (4), the PEMWE voltage $\widetilde{V}_j$ at time instant $k$ can be expressed by the following recurrence relation

$$\widetilde{V}_{j_k} = \sum_{h=0}^{n-1} b_{j_h} \widetilde{I}_{j_{k-n+h}} - \sum_{h=0}^{n-1} a_{j_h} \widetilde{V}_{j_{k-n+h}} + \mathcal{E}_{j_k} + \sum_{h=0}^{n} a_{j_h} \mathcal{E}_{j_{k-n+h}}. \tag{5}$$

To validate the obtained transfer function $F_{d_j}(z)$, the following decorrelation test is applied as proposed in [18], [19]

$$R_N(i) = \frac{\sum_{k=i}^{N} \varepsilon_{j_k} \widehat{V}_{j_{k-i}}}{\left( \sum_{k=1}^{N} \widehat{V}_{j_k}^2 \sum_{k=1}^{N} \varepsilon_{j_k}^2 \right)^{0.5}} \tag{6}$$

where $\varepsilon_j$ is the zero-mean version of $\mathcal{E}_j$ in (4), $N$ is the number of measurement samples and $i = 0, 1, \ldots, n$, with $n = \deg(D_{d_j}(z))$. The identified model is considered valid if

$$|R_N(i)| \leqslant \ell_c = \frac{2.17}{\sqrt{N}} \quad \text{or} \quad |R_N(i)| \leqslant \ell_p = 0.15 \tag{7}$$

In this paper, three operating points are considered (see (3a)):

- 1st operating point: $I_0 = 10\,\text{A}$,
- 2nd operating point: $I_0 = 8\,\text{A}$,
- 3rd operating point: $I_0 = 14\,\text{A}$.

For the identification procedure the same Pseudo Random Binary Sequence (PRBS) excitation is applied to all considered operating points with a magnitude of 4 A, and a sampling period $T_s = 0.001\,\text{s}$. The PRBS signal used for the 1st operating point is shown in Fig. 3. For the 2nd and 3rd operating points, only the current range is changed: 8 A to 12 A and 14 A to 18 A, respectively.

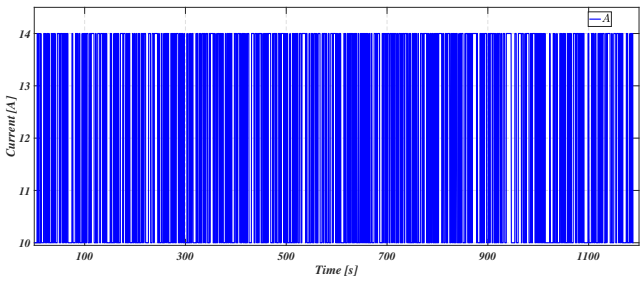


Fig. 3: PRBS current for 1st operating point

Applying the OE identification methods to the three operating points $(j = 1, 2, 3)$ yields the corresponding estimated voltages $V_{OE_j}$. For model orders $n < 5$, the validation criterion given in (6) and (7) fails for the three considered operating points. Hence, a model order of $n = 5$ is retained for $F_{d_j}(z)$. The best models are obtained using Output Error with Adaptive Filtered Observations (OEAFO) method, with variable forgetting factor [19]. Figures 4, 5 and 6 show the measured voltages $V$ compared with the estimated voltages $V_{OE_j}$ where $(j = 1, 2, 3)$. The application of decorrelation test given in (6) and (7) is illustrated in Figures 7, 8 and 9.

For the three operating points, the identified transfer functions are given by (where $F_{d_j}(z) = F_{OE_j}(z)$, see(1))

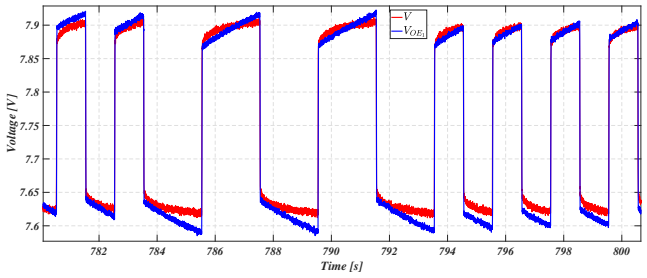


Fig. 4: Measured and estimated voltages $V$ and $V_{OE_1}$ for 1st operating point

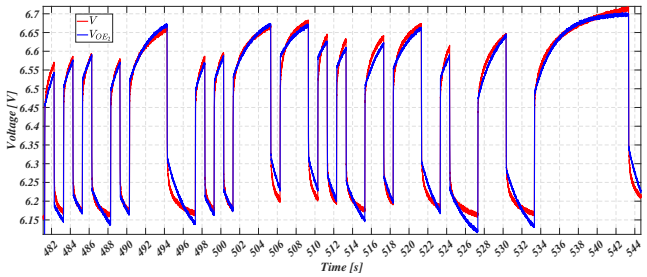


Fig. 5: Measured and estimated voltages $V$ and $V_{OE_2}$ for 2nd operating point

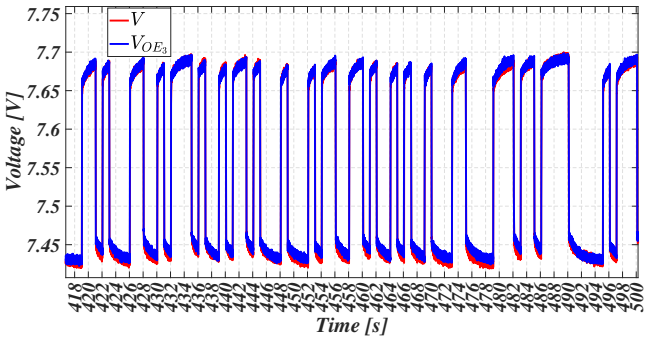


Fig. 6: Measured and estimated voltages $V$ and $V_{OE_3}$ for 3rd operating point

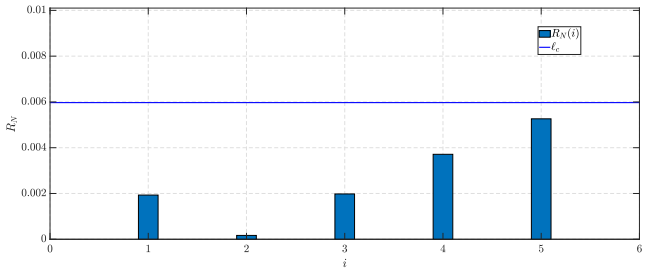


Fig. 7: Decorrelation test for 1st operating point

$$F_{OE_1}(z) = \frac{0.03651z^4 - 0.08377z^3 + 0.0286z^2 + 0.08714z - 0.06846}{z^5 - 0.9181z^4 - 0.9454z^3 + 1.04z^2 - 0.008087z - 0.1682},$$

$$F_{OE_2}(z) = \frac{-0.003881z^4 + 0.03086z^3 + 0.04159z^2 - 0.01328z - 0.05518}{z^5 + 0.4538z^4 - 0.9586z^3 - 1.142z^2 + 0.01602z + 0.6311},$$

$$F_{OE_3}(z) = \frac{0.08227z^4 - 0.1069z^3 + 0.01036z^2 + 0.09637z - 0.08193}{z^5 - 0.7407z^4 - 0.4487z^3 + 0.9967z^2 - 0.4667z - 0.3389}$$

Due to the highly nonlinear behavior of the PEMWE, we

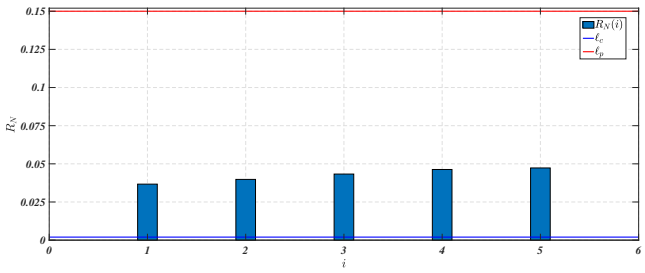


Fig. 8: Decorrelation test for 2nd operating point

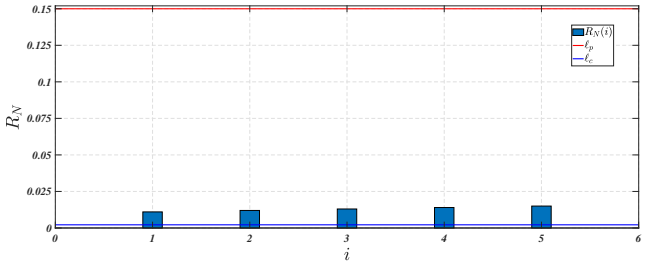


Fig. 9: Decorrelation test for 3rd operating point

can see that its response is not symmetrical when subjected to increasing and decreasing PRBS steps. As a result, the identified models tend to better capture the dynamics during increasing steps than during decreasing ones, which affects the overall quality of the identification procedure. Unlike the 2nd and 3rd operating points (see Fig. 8 and Fig. 9), the 1st operating point validates both $\ell_c$ and $\ell_p$ limits in (7) (see Fig. 7). A step response of the model $F_{OE_1}$ shown in Fig. 10 exhibits both good transient and steady-state behaviors.

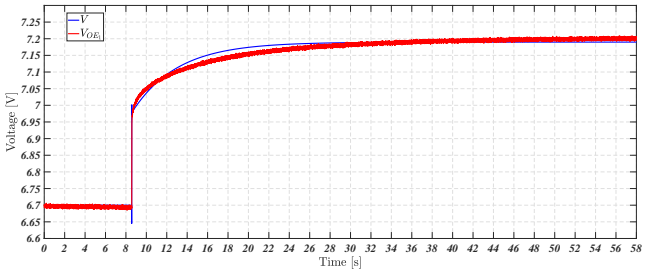


Fig. 10: Step response of $F_{OE_1}$ model

### C. Frequency domain approach

Electrochemical systems are often characterized using Electrochemical Impedance Spectroscopy (EIS) [20], [21]. This method consists in exciting the electrochemical system with a sufficiently wide range of sinusoidal signals around an operating point. If the exciting signal is a current, the method is referred as galvanostatic, while the exciting signal is a voltage, the method is referred as potentiostatic. This approach has been recently applied to PEMWE systems in [13], [14].

In this paper, the galvanostatic approach is applied around an operating point of 15 A, with a frequency range spanning from 10 mHz to 10 kHz and an amplitude of 10% of the

considered operating current point. Each frequency is associated to a complex number characterizing the behavior of the PEMWE system at that frequency. The Bode gain diagram of the obtained experiment is plotted by the red curve in Fig. 11, the experimental Bode phase diagram is shown in Fig. 12 and the experimental Nyquist diagram is presented in Fig. 13, both using red colour.

Using "estimate transfer function" in Matlab (called tfest.m) some continuous time transfer functions are identified from the obtained frequency response data. The following comments can be made

- For transfer functions of order 4 or less, the obtained frequency responses do not match with the experimental data.
- For transfer functions of order 7 or higher, the obtained frequency responses are very close and match satisfactorily with the experimental data.

The identified transfer functions of orders 5, 6 and 7 are given by (8), (9) and (10), respectively, and the corresponding frequency responses are plotted in Fig. 11, Fig. 12 and Fig. 13.

For the identified models of orders 5, 6 and 7, the following comments can be made:

- In the Bode gain diagram shown in Fig. 11, the curves of the three identified models are very close and match very well with experimental data.
- The phase diagram presented in Fig. 12 reveals some differences between the curves of the three identified models. The $7^{\text{th}}$ order model curve provides the best match with the experimental data, while the $5^{\text{th}}$ order curve matches less well.
- The Nyquist diagram shown in Fig. 13 confirms the analysis made from the gain and phase Bode diagrams. It also allows us to discriminate between the $6^{\text{th}}$ and $7^{\text{th}}$ order models. Indeed, although the $7^{\text{th}}$ order model fits slightly better than the $6^{\text{th}}$ order one, both are significantly closer to the experimental data than the $5^{\text{th}}$ order model.

To validate the identified models with the frequency approach, step responses are simulated and plotted in Fig. 14.

The steps responses in Fig. 14 confirm the above frequency domain analysis: the models of orders 6 and 7 are closely aligned with the experimental data, whereas the $5^{\text{th}}$ order model deviates more, particularly in steady-state behavior. Indeed, the steady-state behavior corresponds to the low-frequency response where the model curves of order $5^{\text{th}}$ follow the experimental data least closely as shown in Fig. 12 and Fig. 13.

### *D. Distance between the identified models*

In order to evaluate the obtained identified models from temporal and frequential approaches, the gap metric defined in [22], [23] is used. Let $\mathcal{H}_\infty$ be the set of stable and causal continuous linear time invariant systems [24], [25]. The gap metric between two linear continuous time systems $P_1(s)$ and $P_2(s)$ is called $\delta(P_1, P_2)$ and defined as follows:

$$\delta(P_1,P_2)=\max\left\{\inf_{\Theta(s)\in\mathcal{H}_\infty}\left\|\begin{bmatrix}M_1(s)\\N_1(s)\end{bmatrix}-\begin{bmatrix}M_2(s)\\N_2(s)\end{bmatrix}\Theta(s)\right\|_\infty,\right.$$
$$\left.\inf_{\Theta(s)\in\mathcal{H}_\infty}\left\|\begin{bmatrix}M_2(s)\\N_2(s)\end{bmatrix}-\begin{bmatrix}M_1(s)\\N_1(s)\end{bmatrix}\Theta(s)\right\|_\infty\right\} \quad (11)$$

where $M_i(s), N_i(s)$ are the normalized right coprime factorization in $\mathcal{H}_\infty$ of systems $P_i(s)$, i.e,

$$P_1(s)=N_1(s)M_1^{-1}(s),\quad P_2(s)=N_2(s)M_2^{-1}(s)$$
$$I=N_1^T(-s)N_1(s)+M_1^T(-s)M_1(s)$$
$$I=N_2^T(-s)N_2(s)+M_2^T(-s)M_2(s)$$

The gap metrics between the identified models are given in Table II, where $F^c_{OE_1}(s)$, $F^c_{OE_2}(s)$ and $F^c_{OE_3}(s)$ are continuous time models obtained by applying the bilinear transform to the discrete time models $F_{OE_1}(z)$, $F_{OE_2}(z)$ and $F_{OE_3}(z)$, respectively.

TABLE II: Gap metric between identified models

| $\delta(\times,\times)$ | $F^c_{OE_1}$ | $F^c_{OE_2}$ | $F^c_{OE_3}$ | $F_{EIS_5}$ | $F_{EIS_6}$ | $F_{EIS_7}$ |
|---|---|---|---|---|---|---|
| $F^c_{OE_1}$ | 0 | | | | | |
| $F^c_{OE_2}$ | 0.3 | 0 | | | | |
| $F^c_{OE_3}$ | 0.197 | 0.411 | 0 | | | |
| $F_{EIS_5}$ | 0.138 | 0.266 | 0.173 | 0 | | |
| $F_{EIS_6}$ | 0.137 | 0.267 | 0.172 | 0.00257 | 0 | |
| $F_{EIS_7}$ | 0.137 | 0.267 | 0.172 | 0.00414 | 0.00224 | 0 |

The following comments can be made:

- $F_{EIS_6}(s)$ is the model closest to all others.
- $F^c_{OE_2}(s)$ is the least close to the rest of the models.
- The distance between the identified models using temporal domain approach are of the same order of magnitude.
- The distance between the identified models with the frequency domain approach is of the same order of magnitude.
- The distances between the identified models with frequency approach in the one hand and with temporal approach in other hand are 100 times shorter.

## III. Discussion

This discussion is based on the different approaches applied for PEMWE identification in Section II. The objective is to raise several open questions related to the identification of PEMWE models for control and diagnosis purposes.

**(1) Assessment of the applied identification approaches:**
For the time domain approach, several identification methods have been tested like Auto Regressive and Moving Average with External excitation (ARMAX) and Output Error (OE). The obtained results do not satisfy the criterion given in (7), even for models of reasonable order (slightly higher than 5). The lowest order models have been obtained using a refined OE

$$F_{EIS_5}(s) = \frac{0.02853s^5 + 205.5s^4 + 7.946e04s^3 + 1.512e06s^2 + 3.078e06s + 6.377e05}{s^5 + 4611s^4 + 1.186e06s^3 + 1.564e07s^2 + 2.146e07s + 2.979e06}, \quad (8)$$

$$F_{EIS_6}(s) = \frac{0.02737s^6 + 403s^5 + 4.667e05s^4 + 5.015e07s^3 + 5.068e08s^2 + 6.438e08s + 1.009e08}{s^6 + 1.051e04s^5 + 8.42e06s^4 + 6.784e08s^3 + 4.788e09s^2 + 4.214e09s + 4.684e08}, \quad (9)$$

$$F_{EIS_7}(s) = \frac{0.02752s^7 + 357s^6 + 3.442e05s^5 + 3.009e07s^4 + 3.895e08s^3 + 1.553e09s^2 + 1.339e09s + 1.538e08}{s^7 + 9093s^6 + 6.024e06s^5 + 4.031e08s^4 + 4.183e09s^3 + 1.349e10s^2 + 8.276e09s + 7.066e08} \quad (10)$$

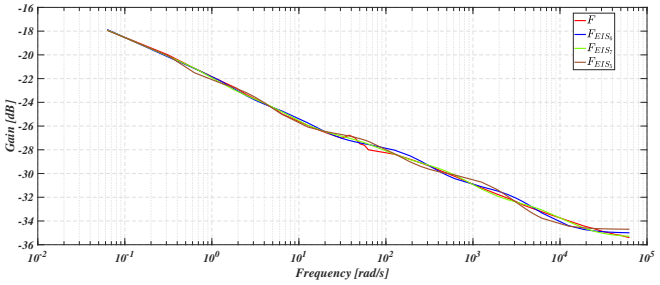


Fig. 11: Bode gain diagrams

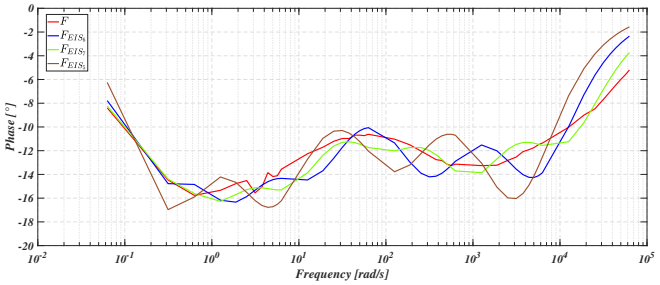


Fig. 12: Bode phase diagrams

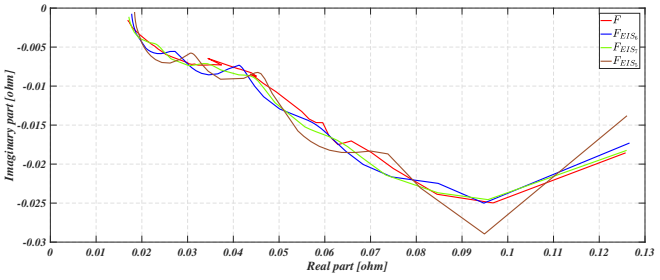


Fig. 13: Nyquist diagrams

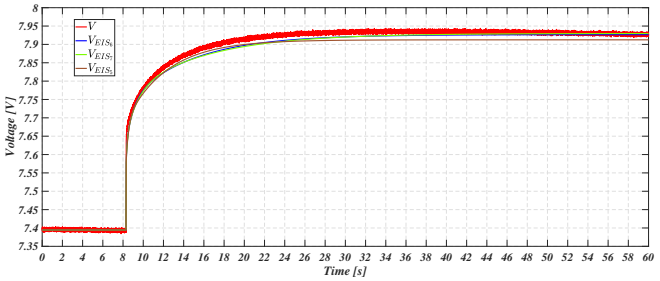


Fig. 14: Step responses for validation

approach, namely the Output Error with Adaptive Filtered Observations (OEAFO) method.

The idea behind using three operating points is to identify models that cover a sufficiently large operating range of the PEMWE. The choice of this operating range depends on the intended application of the PEMWE.

For the frequency domain approach, the EIS method, widely employed in electrochemical processes, is considered. Models identification are carried out using the Matlab function "tfest.m". For low-order models (order less than 4), a significant deviations are observed compared to the experimental frequency data. For higher order models (order greater than 7), no improvement is observed beyond the 7$^{\text{th}}$ order.

The gap metric approach has been used to determine the most "central" model which could be used for both control and diagnosis purposes.

**(2) Relevance of the operating points selection:**

The identification results reveal noticeable differences between the models obtained at the three operating points. This suggests that the PEMWE exhibits nonlinear behavior over its operating range, and that each model captures only local dynamics specific to its operating condition. Consequently, the choice of operating points is crucial for constructing models that are representative of the system under varying conditions. From a practical perspective, this observation raises the question of whether a single linear model is sufficient for control and/or diagnosis tasks, or whether a gain-scheduled or piecewise linear modeling approach would be more appropriate.

Identifying the most representative operating points—based on specific usage profiles of the PEMWE—thus becomes a key aspect of the modeling strategy.

**(3) High model order and aging-related complexity:**

Compared to the models typically reported in the literature for PEMWE systems, the identified models exhibit significantly higher orders. This difference could arise from multiple factors, including the lack of tight control over the operating conditions during the identification experiments, or from the intrinsic characteristics of the tested PEMWE stack.

One plausible explanation is the effect of aging. As the PEMWE degrades over time, not only do its phys-

ical parameters change, but its internal dynamics may become more complex. This complexity can manifest as an apparent increase in system order meaning that the system requires a higher order model to accurately reproduce its input-output behavior. This insight suggests that degradation affects more than just parameter values: it can also introduce new dynamics.

These observations highlight the importance of taking into account the impact of aging in identification and modeling of the process.

**(4) Control and diagnosis: robustness and heuristics controllers and renewable energy sources (RES):** The identified models serve as a foundation for both control design, health monitoring and diagnosis purposes. From a control point of view, the variability observed across operating points and the high order of the models highlight the need for robust control strategies that can tolerate model uncertainties and potential aging effects. Classical controllers may lack the flexibility to adapt to such variations, suggesting the use of robust control strategies (e.g., $\mathcal{H}_\infty$, adaptive control) or data-driven or model-free or PID control approaches "heuristic-based methods" (e.g., fuzzy logic, neural networks, or reinforcement learning) as complementary or alternative solutions.

In terms of diagnosis, reliable models can enhance fault detection and isolation by enabling the comparison between measured and estimated signals, thus improving system observability and the ability to distinguish between normal behavior and degradation.

Additionally, the integration of PEMWE systems with Renewable Energy Sources (RES) requires models capable of handling dynamic and intermittent operating conditions. This adds another layer of complexity that should be taken into account during the modeling or identification phases to ensure compatibility with energy management strategies and real-time control.

## IV. Conclusion

The identification of an experimental PEMWE system has been addressed using both temporal and frequency domains approaches. Due to the strong nonlinearities of the PEMWE process, several operating points were considered in order to identify multiple linear models that can describe the system's behavior over a wide operating range. The identified models have an order between 5 and 7, which is higher than those commonly reported in the literature. The obtained results have raised several open questions: operating points selection, aging-related complexity, control and diagnosis applications.

## References


[1] S. Sharshir, A. Joseph, M. Elsayad, A. Tareemi, A. Kandeal, and M. Elkadeem, "A review of recent advances in alkaline electrolyzer for green hydrogen production: performance improvement and applications," *Int. J. of Hydrogen Energy*, vol. 49, pp. 458–488, 2023.

[2] D. Falcão and A. Pinto, "A review on PEM electrolyzer modelling: guidelines for beginners," *J. Cleaner Production*, vol. 261, p. ID 121184, 2020.

[3] C. Li and J. Baek, "The promise of hydrogen production from alkaline anion exchange membrane electrolyzers," *Nano Energy*, vol. 87, p. ID 106162, 2021.

[4] R. Keller, E. Rauls, M. Hehemann, M. Müller, and M. Carmo, "An adaptive model-based feedforward temperature control of a 100 kW PEM electrolyzer," *Control Engineering Practice*, vol. 120, p. ID 104992, 2022.

[5] P. Olivier, C. Bourasseau, and B. Bouamama, "Low-temperature electrolysis system modelling: a review," *Renewable and Sustainable Energy Reviews*, vol. 78, pp. 280–300, 2017.

[6] M. Agredano-Torres, M. Zhang, L. Söder, and Q. Xu, "Decentralized dynamic power sharing control for frequency regulation using hybrid hydrogen electrolyzer systems," *IEEE Trans. Sustainable Energy*, vol. 15, pp. 1847–1858, 2024.

[7] Á.. Hernández-Gómez, V. Ramirez, and D. Guilbert, "Investigation of PEM electrolyzer modeling: electrical domain, efficiency, and specific energy consumption," *Int. J. of Hydrogen Energy*, vol. 45, pp. 14625–14639, 2020.

[8] F. Alonge, S. Collura, F. D'Ippolito, D. Guilbert, M. Luna, and G. Vitale, "Design of a robust controller for DC/DC converter-electrolyzer systems supplied by $\mu$WECSs subject to highly fluctuating wind speed," *Control Engineering Practice*, vol. 98, p. ID 104383, 2020.

[9] M. Şahin, H. Okumuş, and M. Aydemiri, "Implementation of an electrolysis system with DC/DC synchronous buck converter," *Int. J. of Hydrogen Energy*, vol. 39, pp. 6802–6812, 2014.

[10] D. Guilbert, M. Zasadzinski, H. Rafaralahy, and L. Boutat-Baddas, "Modeling of the dynamic behavior of a PEM electrolyzer," in *Proc. IEEE Int. Conf. on Systems and Control*, (Marseille, France), 2022.

[11] R. Maamouri, D. Guilbert, M. Zasadzinski, and H. Rafaralahy, "Proton exchange membrane water electrolysis: modeling for hydrogen flow rate control," *Int. J. of Hydrogen Energy*, vol. 46, pp. 7676–7700, 2021.

[12] M. Khalid Ratib, K. Muttaqi, M. Islam, D. Sutanto, and A. Agalgaonkar, "Electrical circuit modeling of proton exchange membrane electrolyzer: the state-of-the-art, current challenges, and recommendations," *Int. J. of Hydrogen Energy*, vol. 49, pp. 625–645, 2024.

[13] T. Miličić, K. Muthunayakage, T. Hoàng Vũ, T. Ritschel, L. Živković, and T. Vidaković-Koch, "The nonlinear frequency response method for the diagnosis of PEM water electrolyzer performance," *Chemical Engineering J.*, vol. 496, p. ID 153889, 2024.

[14] D. Brinker, N. Hensle, J. Horstmann de la Viña, I. Franzetti, L. Bühre, U. Andaluri, C. Menke, T. Smolinka, and A. Weber, "Inductive loops in impedance spectra of PEM water electrolyzers," *J. of Power Sources*, vol. 622, p. ID 235375, 2024.

[15] A. Makhsoos, M. Kandidayeni, M. Ait Ziane, L. Boulon, and B. Pllet, "Model benchmarking for PEM water electrolyzer for energy management purposes," *Energy Conversion and Management*, vol. 323, p. ID 119203, 2025.

[16] L. Ljung, *System Identification: Theory for the User*. Englewood Cliffs, New Jersey: Prentice Hall, 1987.

[17] T. Söderström and P. Stoica, *System Identification*. Englewood Cliffs, New Jersey: Prentice Hall, 1989.

[18] I. Landau, *System Identification and Control Design*. Englewood Cliffs, New Jersey: Prentice Hall, 1990.

[19] I. D. Landau and G. Zito, *Digital Control Systems -Design, Identification and Implementation*. Communication and Control Engineering, Springer, London, Sept. 2009.

[20] T. Vidaković-Koch, T. Miličić, L. Živković, H. Seng Chan, U. Krewer, and M. Petkovska, "Nonlinear frequency response analysis: a recent review and perspectives," *Current Opinion in Electrochemistry*, vol. 30, p. ID 100851, 2021.

[21] T. Miličić, M. Sivasankaran, C. Blümner, A. Sorrentino, and T. Vidaković-Koch, "Pulsed electrolysis – explained," *Faraday Discussions*, vol. 246, pp. 179–197, 2023.

[22] T. Georgiou, "On the computation of the gap metric," *Syst. & Contr. Letters*, vol. 11, pp. 253–257, 1988.

[23] T. Georgiou and M. Smith, "Optimal robustness in the gap metric," *IEEE Trans. Aut. Control*, vol. 35, pp. 673–686, 1990.

[24] M. Vidyasagar, *Control System Synthesis: A Factorization Approach*. Cambridge, USA: MIT Press, 1985.

[25] B. Francis, *A Course in $\mathcal{H}_\infty$ Control Theory*, vol. 88 of *Lecture Notes in Control and Information Sciences*. New York: Springer-Verlag, 1987.